ARTICLE

OPEN

Check for updates

A fully planar solar pumped laser based on a luminescent solar collector

Taizo Masuda[1✉], Mitsuhiro Iyoda[2], Yuta Yasumatsu[2], Stephan Dottermusch[3], Ian A. Howard [3,4],
Bryce S. Richards[3,4], Jean-Francois Bisson [2,5] & Masamori Endo[2]

A solar-pumped laser (SPL) that converts sunlight directly into a coherent and intense laser beam generally requires a large concentrating lens and precise solar tracking, thereby limiting its potential utility. Here, we demonstrate a fully-planar SPL without a lens or solar tracking. A Nd^{3+}-doped silica fiber is coiled into a cylindrical chamber filled with a sensitizer solution, which acts as a luminescent solar collector. The body of the chamber is highly reflective while the top window is a dichroic mirror that transmits incoming sunlight and traps the fluorescence emitted by the sensitizer. The laser-oscillation threshold was reached at a natural sunlight illumination of 60% on the top window. Calculations indicated that a solar-to-laser power-conversion efficiency could eventually reach 8%. Such an SPL has potential applications in long-term renewable-energy storage or decentralised power supplies for electric vehicles and Internet-of-Things devices.

[1] S-Frontier Division, Toyota Motor Corporation, Susono, Shizuoka, Japan. [2] Department of Physics, Tokai University, Hiratsuka, Kanagawa, Japan. [3] Institute of Microstructure Technology, Karlsruhe Institute of Technology, Hermann-von-Helmholtz-Platz 1, 76344 Eggenstein-Leopoldshafen, Germany. [4] Light Technology Institute, Karlsruhe Institute of Technology, Engesserstrasse 13, 76131 Karlsruhe, Germany. [5] Département de physique et d'astronomie, Université de Moncton, 18 Antonine-Maillet, Moncton, NB E1A 3E9, Canada. ✉email: taizo_masuda@mail.toyota.co.jp

Solar-pumped lasers (SPLs), which convert sunlight into laser radiation, are of interest for applications, such as solar hydrogen generation, remote area telecommunications, space propulsion, space solar power systems, and high-efficiency photovoltaic energy conversion[1–8]. In addition, SPLs could play a critical role in a more sustainable magnesium energy cycle, reconverting magnesium oxide to magnesium[2,9,10]. Although many improvements in the optical gain medium and solar collector design have been reported since the first demonstration of an SPL[11], most SPLs still rely on lens or mirror concentrator systems with concentration factors on the order of thousands to obtain sufficient gain in the irradiated active medium[12–18]. Such concentration optics limit the practicality of SPLs because they are expensive and require very precise tracking of the sun to keep the focal point on the active medium to within 0.01°[19], which is challenging at high winds. The system is thus unwieldy, and both the capital and operational costs are prohibitive. In addition, realizing optical concentration via lenses and/or mirrors can only be achieved using direct beams of sunlight; it is not possible when the diffuse component of sunlight is high (for example, in cloudy conditions). Since the diffused component is ~20%, even when the sky is clear and the sun is very high in the sky, and it is >50% on average[20], it is highly beneficial for solar energy conversion devices to utilize both direct and diffused components. These factors constrain the practical applications of SPLs that rely on lens or mirror concentrator systems[12,13,17,21]. Reductions in the size and weight of SPLs to a scale comparable to that of photovoltaic (PV) panels would open up new applications for SPLs because a flat-plate device is suitable not only to large scale applications, but also to small scale ones[22]. For example, a flat-plate SPL system could be used for wireless power feeding to electric vehicles[23–25] and unmanned aerial vehicles[26].

To dramatically reduce the required concentration factor to overcome the drawbacks of conventional SPLs, a cascade energy transfer by a sensitizer was reported[13]. Although this scheme successfully reduced the lasing threshold to 230 suns, the system still required a lens/mirror concentrator to achieve lasing. We previously demonstrated an SPL using a fiber laser with transverse excitation geometry combined with cascade energy transfer in a narrow circular-shaped chamber, which contained sensitizer solution[27]. A 40-m-long Nd^{3+}-doped fiber was circularly coiled inside a chamber with a width of 5 mm, a height of 1 mm, and a diameter of 300 mm. Sunlight was concentrated via a toroidal lens with a 580-mm outer diameter to form a focal shape of a thin-ring whose diameter is the same as that of the coiled fiber. This laser operated under natural sunlight and relied on an extremely low solar concentration of only 1.5 W cm^{-2} (15 suns) illuminated on the active medium; however, the system still relied on a lens and a solar tracking system[27].

In this study, we demonstrate lasing in a fully planar SPL without any lens using a luminescent solar collector (LSC) combined with a fiber laser with transverse excitation geometry under natural sunlight. The developed plate-like proof-of-concept SPL system required a sunlight intensity of 0.06 W cm^{-2} illumination on the front window of the planar system, which is 60% of the standard air-mass 1.5 global (AM1.5 G) sunlight intensity, to achieve lasing. The maximum output-power value was 1.3 mW when an output coupler with 80% was used. In principle, the solar-to-laser energy conversion efficiency could reach 8% based on the proposed geometry with simple modifications. In addition, the transverse pumping geometry gives SPLs unmatched potential power scalability; once the threshold of laser oscillation is exceeded, the gain value per unit length exceeds the losses, and the output-power scales linearly with fiber length with a marginal cost increase. In contrast, power scaling for a lens or mirror concentrator-based SPL necessitates larger optical elements, whose cost rapidly increases with size. We believe that the developed device constitutes a significant step towards the utilization of SPLs in a wide range of energy conversion applications. The device is planar and passive, and can be easily scaled up without loss of beam quality by connecting modules in series.

Results

Small-signal gain measurements. A cross-sectional schematic diagram of the proof-of-concept solar-pumped fiber laser with a liquid-phase LSC combined with transverse excitation geometry is shown in Fig. 1a and a photograph of the SPL system is shown in Fig. 1b. A photograph of the setup during outdoor measurements is presented in Supplementary Fig. 1. The dye (rhodamine 6G: R6G) dissolved in methanol solution strongly absorbs sunlight between 450 and 550 nm, and its luminescence centred at ~590 nm spectrum matches well the $^4G_{5/2}$-$^4G_{7/2}$ absorption band of the Nd^{3+} ions of the fiber core. The photoluminescence from R6G is confined by the highly reflective (HR) chamber wall and front dichroic window, causing the trapped Stokes-shifted light to bounce back and forth inside the chamber, where the active fiber is bundled, until it is absorbed by the laser medium. The SPL is cooled to below −25 °C to avoid losses caused by thermally excited states in Nd^{3+} and to obtain consistent data under outdoor conditions for the proof-of-concept[28].

The LSC boosts the small-signal gain by a factor of >30 compared to that in a system without the LSC. Based on our previous results obtained with a toroidal lens[27], this gain is appropriate for realizing solar-powered lasing without a lens or mirror concentrator.

The measured small-signal gain per pass as a function of solar irradiance is given in Fig. 2a, where the solar irradiance was varied by shading the LSC illuminated by natural sunlight with an iris composed of black pie-shaped plates (see Supplementary Fig. 1). It can be seen that the observed small-signal gain is proportional to the solar irradiance. Figure 2b shows the measured small-signal gain spectrum under natural sunlight
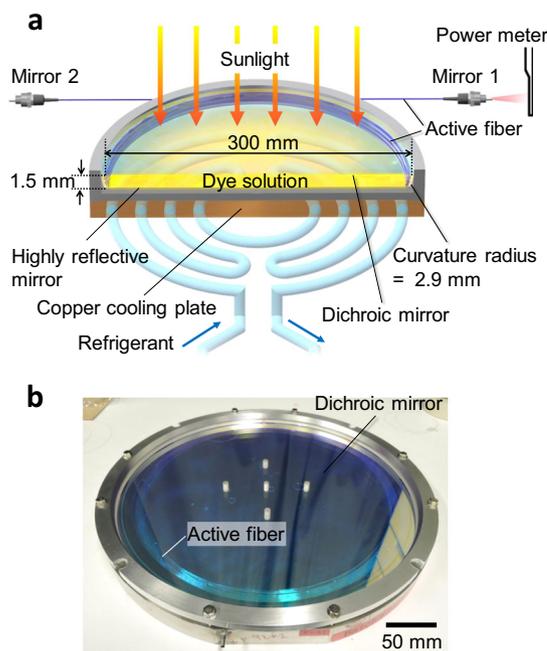

Fig. 1 Fully planar solar-pumped laser geometry without lens/mirror concentrator and tracking system. a Schematic cross-sectional diagram of a solar-pumped fiber laser with luminescent solar collector. **b** Photograph of the solar-pumped fiber laser.
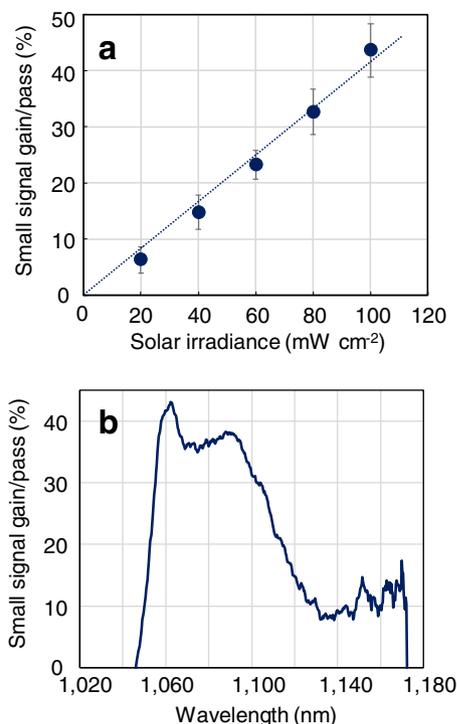
Fig. 2 Small-signal gain measurements under natural solar irradiance. a Measured small-signal gain per pass as a function of solar irradiance at $\lambda = 1064$ nm. The solar irradiance was varied by shading the luminescent solar collector with black fan-shaped plates. The error bars in this figure represent the statistical errors in the measurements. **b** Measured small-signal gain spectrum, showing a peak at 1064 nm. The emission wavelength range of the superluminescent was 1045 to 1170 nm.

Fig. 3 Measurement results of laser performance at −45 °C. a Measured output power as a function of solar irradiance. The error bars in this figure represent the statistical errors in the measurements. **b** Measured output emission spectrum of the solar-pumped fiber laser with reflectance of 90% for the output coupler under 1 sun (i.e., 100 mW cm^{-2}) condition.

without the iris (0.1 W cm^{-2}), demonstrating a very wide gain bandwidth range of 1050 to 1130 nm. The measured peak small-signal gain was 44% per pass of 190-m long fiber (8.4 dB km^{-1}) at 1064 nm. Since the base loss of the fiber at the gain band is 12% per pass (3 dB km^{-1}) and the reflection loss of the end mirror (pigtail reflector) is 1.5%[27–29], the observed gain is sufficient to achieve lasing.

Laser-characteristic measurements. We then investigated the laser characteristics using six reflectance values ($R = 99\%$, 95%, 90%, 80%, 70%, and 50%) for the output coupler (mirror 1). The measured laser output power as a function of solar irradiance is given in Fig. 3a. The obtained maximum output power was 1.3 mW at $R = 80\%$ under natural solar irradiance without the iris. No laser action was observed with $R = 50\%$. The measured smallest lasing threshold was 0.06 W cm^{-2} (60% of natural sunlight intensity) illuminated on the front window of the planar system when the reflection of the output coupler was 99%. Figure 3b shows the measured output emission spectrum of the SPL with a reflectance of 90% for the output coupler. Several oscillation peaks appear between 1085 and 1100 nm, which were independent of reflectance values as shown in Supplementary Figure 2. The reason for this multi-peak emission is given in the Supplementary Notes 1 (see Supplementary Figs. 3 and 4).

These results demonstrate, for the first time, an SPL that operates without a lens/mirror-based concentrator system usually required for SPLs[14–18,25]. Since the irradiance of the front surface of the SPL was ~70 W, the solar-to-laser conversion efficiency was only 1.8×10^{-5}. Although the observed laser output power is still low (due to the low volume ratio of the fiber core in the LSC and low reflection of the chamber sidewall), the developed fully planar
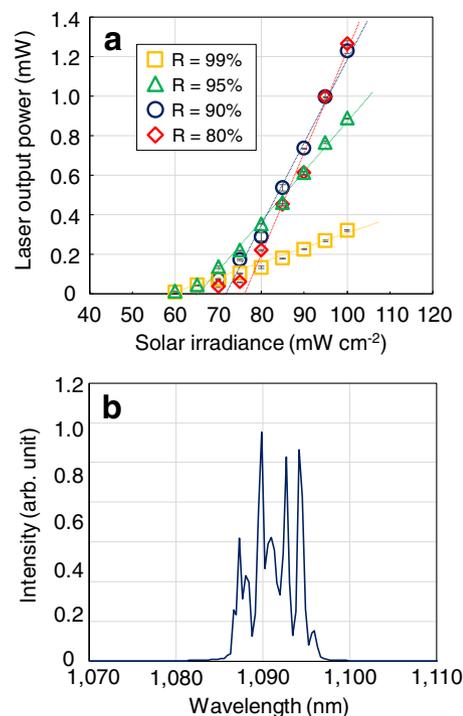
and passive SPL system has the potential to achieve efficiency comparable to that of conventional SPLs, as we will show in the next section. Moreover, the proposed transverse pumping configuration provides, in principle, unlimited power scalability, which is implemented by increasing the fiber length and expanding the surface area of the LSC at the same time.

Discussion
The laser emission spectrum, shown in Fig. 3b, ranges between 1085 and 1100 nm. This is red-shifted compared to the peak value of the small-signal gain at 1064 nm (Fig. 2b). The small-signal gain shown in Fig. 2a, b is a differential gain, defined as the difference between gains measured with and without solar illumination. The gain spectrum, $\gamma(\lambda)$, is given by the following equation:

$$\gamma(\lambda) = N_2\sigma_e(\lambda) - N_1\sigma_a(\lambda) - \alpha_{BG} \qquad (1)$$

where N_1 and N_2 are the populations of the lower ($^4I_{11/2}$) and upper ($^4F_{3/2}$) laser levels in the Nd^{3+} system, respectively; $\sigma_e(\lambda)$ and $\sigma_a(\lambda)$ are the effective emission and absorption cross-sections of Nd^{3+}, respectively; α_{BG} represents background losses. As the saturated and unsaturated losses are almost unchanged via solar illumination, the signal shown in Fig. 2a, b is proportional to $\sigma_e(\lambda)$. For $\gamma(\lambda)$ calculated using the measured $\sigma_e(\lambda)$ and $\sigma_a(\lambda)$ spectra, the threshold gain is reached at ~1090 nm even though σ_e is maximal at 1064 nm, because σ_a is larger towards the shorter-wavelength end of the spectrum[28]. The calculated gain curves are given in Supplementary Figs. 3 and 4. A blue-shift is expected to occur when the medium is cooled; however, we identified that the output emission spectrum was independent of the temperature, as shown in Supplementary Fig. 5. This can be explained by the fact that the number density in the upper laser level was not adequately high to enable us to observe the blue-shifted emission.

As we have acquired laser outputs at several different out-coupling mirrors, we attempted Rigrod analysis[30] for this set of outputs vs. mirror transmittance. Since we have all of the measured values that are necessary for the analysis other than the saturation intensity, the analysis aims to identify the saturation intensity that draws the curve closest to the experimental data. However, the well-known method reported by Rigrod[30] for high-gain lasers is correct only under the approximation that the gain per unit length is sufficiently larger compared to the distributed loss per unit length. Since the small-signal gain coefficient is smaller than three times of the loss factor in the prototype laser system, this approximation does not apply.

When considering a one-dimensional optical resonator along the z-axis with a homogeneously broadened laser medium having a small-signal gain coefficient g_0 and loss coefficient α_0, the one-way optical intensity at any z obeys the following ordinary differential equation[31]:

$$\frac{d\beta_+}{dz} = \frac{\beta_+[(g_0 - \alpha_0)\beta_+ - \alpha_0(\beta_+^2 + \beta_0^2)]}{[\beta_+^2 + \beta_+ + \beta_0^2]} \quad (2)$$

where $\beta_+ = I_+(z)/I_s$ and $\beta_- = I_-(z)/I_s$ are normalized optical intensity in the $+z$ and $-z$ directions, respectively, with respect to the saturation intensity I_s; and $\beta_0 = \beta_+\beta_-$ is independent of z.

Although Eq. (2) can be integrated analytically, the result does not help to obtain the laser output directly because it contains β_0. Instead, we used $\beta_0 = \beta_1^2/r_1$, where β_1 is the normalized forward intensity at $z = 0$, and r_1 is the reflectivity of the resonator mirror placed at $z = 0$. Substituting this into Eq. (2), it can be numerically integrated, and output power is obtained by:

$$P_{out} = I_s A \beta_2 (1 - r_2 - a) \quad (3)$$

where β_2 is the normalized forward intensity at the right-hand end of the medium; r_2 is the right-hand side mirror reflectivity; and a is the reflection loss at the mirror. Further details are given in the literature[32].

Figure 4 presents a comparison between the Rigrod curve and the experimental results when $g_0 = 1.92 \times 10^{-3}$ m^{-1} (44%/pass), $a = 1.5\%$[29], $\alpha_0 = 6.91 \times 10^{-4}$ m^{-1} (3 dB km^{-1})[27], the medium length is 190 m, and the medium cross-section is a circle with 16 μm diameter. The calculation was carried out by varying I_s, and the Rigrod curve agrees very well with the experimental results when I_s set to 14 kW cm^{-2}. Therefore, it was shown that the observed laser power vs. output coupling coefficient could be well explained by the known characteristics of the laser medium and the optical resonator.

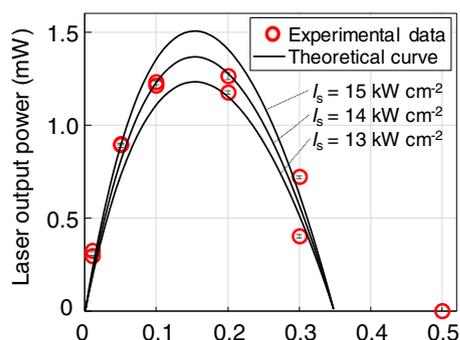Finally, we calculated the physical properties of the developed planar SPL device in order to estimate the attainable conversion efficiency of the developed system by a developed Monte Carlo simulation code[33]. Details of the simulation method are presented in the Supplementary Notes 2 (see Supplementary Fig. 6). The code simulates a structure in which a fiber is wound near the circumference of a cylindrical case, the top surface is a dichroic mirror (DM), and the bottom surface is an HR wall, as illustrated in Fig. 5. Since the reflection of the sidewall cannot be measured due to its curved nature, the reflectance is a fitting parameter that is adjusted to match the experimental results. The calculated small-signal gains are in good agreement with the experimental results when the sidewall reflection value is set to 45%, as shown in Supplementary Fig. 7.

We calculated the laser output-power values after making some modifications to the developed SPL device. In the current SPL prototype, only 0.04% of the incident photons are absorbed by the Nd^{3+} ions in the fiber-core bundle. The biggest loss channel in the current setup is reflection loss at the sidewall (55% per reflection). As shown in Supplementary Fig. 8, the laser output-power logarithmically increases when the sidewall reflectivity increases. The small core volume of the active fiber in the LSC (i.e., the core diameter is 16 μm, and the fiber length is 190 m) also contributed to inefficient energy transfer to the active medium. The calculations indicate that the solar-to-laser conversion efficiency will reach 1.1% or 11 W m^{-2}, if the sidewall reflectivity is set to 99% and the fiber length is extended to 12 km, as shown in Supplementary Fig. 9.

Furthermore, changing the peak emission wavelength of a sensitizer from visible region to near-infrared (near the $^4F_{5/2}$ absorption band of Nd^{3+}), and increasing its quantum yield near 100% could yield up to an additional seven-fold increase in the solar-to-laser efficiency, as shown in Supplementary Fig. 10. Such sensitizer, namely, formamide lead iodide perovskite quantum dot (QD), has recently been successfully synthesized[34]. We are currently working on these materials[35–37].

Considering the fact that the wall-plug efficiency of commercially available laser diode (LD)-pumped fiber lasers is ~30–40% and the efficiency of PV panels is 20%, the resulting 6–8% efficiency is comparable to the expected efficiency of our laser (8%) under the QD-based condition, but our design is significantly simpler, as it makes it possible to bypass both the PV and LD stages. Therefore, simply increasing the sidewall reflectivity and the active fiber length with QD gives our passive SPL potential as a disruptive technology.

In summary, we demonstrated the lasing of a fully planar SPL without the need for any lens or solar tracking by employing an LSC combined with a fiber laser with transverse excitation
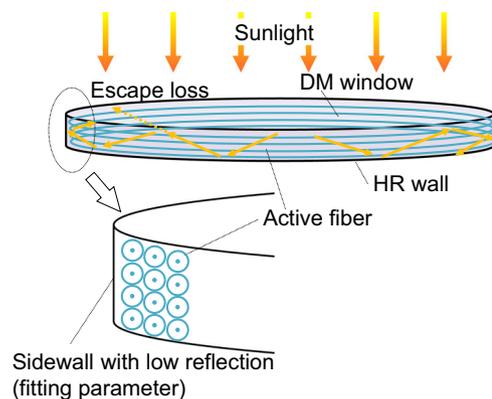

Fig. 4 Measurement results of laser output power as a function of transmittance of the output couplers under 1 sun (i.e., 100 mW cm^{-2}) condition (red circle). The solid curve represents a theoretical curve with different saturation intensity (I_s) values. The error bars in this figure represent the statistical errors in the measurements.

Fig. 5 Schematic diagram of the Monte Carlo simulation for the fully planar solar-pumped laser. The shape of the calculation domain is a plane cylinder, whose top and bottom surfaces represent the dichroic mirror (DM) and highly reflective (HR) mirror, respectively.

geometry. The developed plate-like proof-of-concept SPL system required a sunlight intensity of 0.06 W cm^{-2} illuminated on the front window of the planar system, which is 60% of the standard AM1.5 G sunlight intensity, to achieve lasing. The maximum output power was 1.3 mW at an output coupler with 80% reflectivity. Our numerical calculations suggest that the solar-to-laser conversion efficiency could reach 8% based on the proposed geometry with simple modifications and utilization of the per-ovskite QD, which is comparable to the commercially available fiber laser powered by PV panels. In addition, the transverse pumping geometry gives the proposed SPL unmatched potential power scalability. Once the gain value per unit length exceeds the losses, the output-power scales linearly with fiber length with a marginal cost increase. We believe that the proposed device constitutes a significant step towards the utilization of SPLs for applications, such as solar hydrogen generation and wireless energy feeding to vehicles.

Methods

Fully planar SPL system. The prototype planar SPL system used a Nd^{3+}-doped silica fiber with a 16-μm-diameter core and a 0.18 numerical aperture (Furukawa Electric Co., Ltd.) as the laser medium. The dopant concentration was 0.5 at% that was selected to be the highest, which can keep the low intrinsic loss of the fiber; thus, the value is one order of magnitude larger than that of typical fiber lasers[38]. The absorption spectrum of the active fiber is shown in Fig. 6. The measured peak absorption coefficient of the fiber at 582 nm is 1700 dB m^{-1}. A 190-m-long, circularly coiled fiber was placed in a cylinder-shaped chamber, which functioned as an LSC. The LSC (height: 1.5 mm; diameter: 300 mm) was filled with a solution containing 0.3 mmol L^{-1} of R6G (Sigma Aldrich) in methanol. The bundled fiber was arranged near the sidewall of the chamber. The sidewall had a curvature radius (CR) of 2.9 mm. The LSC was cooled to below −25 °C by a copper cooling plate chilled by a dry ice-methanol refrigerant, which was attached to the bottom surface of the chamber to reduce losses arising from the thermally excited population of the lower laser level and obtain consistent data under outdoor conditions for the proof-of-concept[28]. The gain curve remained almost unchanged when the temperature was lowered, which indicates that the effective cross-sections barely change with temperature[28]. We believe that the cooling system used in this study is required only for the proof-of concept, and it is not an essential restriction for fully planar SPL systems because it would oscillate at room temperature if the rate of photon absorption per unit volume by the active fiber was doubled. The modifications to improve the solar-to-fiber energy transfer have already been discussed in the previous section.

A Piranha etch (H$_2$SO$_4$/H$_2$O$_2$) was used for removing the resin coating of the active fiber to enable more efficient transverse optical excitation. Figure 6 shows the emission and absorption spectra of the dye used in the LSC. The emission peak of the dye is ~590 nm, which matches the $^4G_{5/2}$-$^2G_{7/2}$ absorption band of the Nd^{3+} ion. A high-pass DM with a 570-nm cutoff was coated on the top window of the chamber, as shown in Fig. 6, and the side and bottom walls were coated with a broadband HR mirror, which was made of multiple dielectric layers. Since the dielectric layers deposited on the sidewall had a thickness different from that of those on the bottom face due to the curvature radius, the reflection of the sidewall was smaller than that of the bottom face. Light emitted from the dye was guided
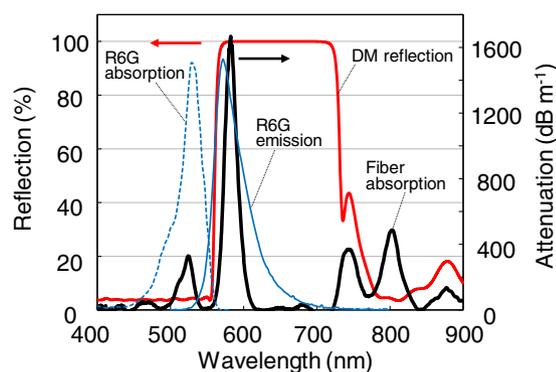
towards the sidewall of the chamber, typically undergoing 2.0 dye interactions, on average, resulting in a slight red-shift (~40 nm) of the R6G emission peak. Overall, the gain per unit length was boosted by a factor of >30 compared to the gain obtained without the sensitizer.

The active fiber was extended outside of the plane cylinder chamber by 2 m in both directions. The two ends of the active fiber were terminated with FC-type connectors using a fiber-end connectorization and polishing kit (Thorlabs, CK05), and contacted to a dielectric-coated bulk mirror (pigtail reflector)[29]. For the output coupler side (mirror 1), several mirrors with reflectance values varying from 99% to 50% designed for laser-diode-pumped Nd:YAG lasers, were used to investigate the laser characteristics. The mirrors were purchased from CVI Laser Optics (PR1-1064-95-1025, PR1-1064-90-1025, PR1-1064-80-1025, PR1-1064-70-1025, PR1-1064-50-1025) and Layertec (Output Coupler #104132). The other side of the mirror (mirror 2) had an HR coating, which was purchased from Autex (PRC-1080-05).

Measurement and data analysis. A superluminescent diode (SLD; Thorlabs S5FC1050P) emitting broadband radiation from 950 to 1170 nm, centred at 1050 nm, was used for small-signal differential gain measurements. The output emission peak measurement was performed by a fiber-coupled near-infrared spectrometer with a resolution of 0.65 nm (Ocean Optics NIRQuest 512 1.7), and laser output power was measured by an optical power meter (Advantest Q82017A). A pyranometer (EKO MS-602) was used for measurements of the solar irradiation illuminated on the front window of the planar system. The measured solar irradiance of natural sunlight was ~100 mW cm^{-2}.

Small signal differential gain coefficient $\gamma(\lambda)$ was calculated as follows:

$$\gamma(\lambda) = \frac{1}{L}\ln\left(\frac{T_1(\lambda)}{T_2(\lambda)}\right) \qquad (4)$$

where $T_1(\lambda)$ and $T_2(\lambda)$ are the measured transmitted spectra of the SLD with and without solar illumination, respectively; and L is the length of the fiber. A significant amount of luminescence was produced by the excited Nd^{3+} ions, which masked the SLD T_1 signal. This luminescence signal was subtracted in the calculations after being separately measured with the SLD turned off.

Data availability

The raw experimental data are available from the corresponding authors upon reasonable request.

Code availability

The computer code is available from the corresponding author upon reasonable request.

Fig. 6 Important data relevant to the simulation code of the luminescent solar collector. Reflectance spectrum of the dichroic mirror, absorption and emission spectra of R6G (arbitrary unit), and fiber absorption coefficient (dB km^{-1}).

References

1. Hisatomi, T. & Domen, K. Reaction systems for solar hydrogen production via water splitting with particulate semiconductor photocatalysts. *Nat. Catal.* **2**, 387–399 (2019).
2. Graham-Rowe, D. Solar-powered lasers. *Nat. Photon.* **4**, 64–65 (2010).
3. Levchenko, I., Bazaka, K., Mazouffre, S. & Xu, S. Prospects and physical mechanisms for photonic space propulsion. *Nat. Photon.* **12**, 649–657 (2018).
4. Editorial. Across the universe. *Nat. Mater.* **17**, 845 (2018).
5. Zhao, Y., Sun, Y., He, Y., Yu, S. & Dong, J. Design and fabrication of six-volt vertically-stacked GaAs photovoltaic power converter. *Sci. Rep.* **6**, 38044 (2016).
6. Takeda, Y. et al. Silicon photovoltaic cells coupled with solar-pumped fiber lasers emitting at 1064 nm. *J. Appl. Phys.* **116**, 014501 (2014).
7. Goto, D., Yoshida, H., Suzuki, H., Kisara, K. & Ohashi, K. The overview of jaxa laser energy transmission r&d activities and the orbital experiments concept on iss-jem. *International Conference on Space Optical Systems and Applications (ICSOS)* S5-2 (Kobe, Japan, 2014).
8. Torres-Soto, L. & Summerer, L. Power to survive the lunar night: and sps application? *Proc. 59th IAC* **IAC-08-C**, 3.1.2 (2008).
9. Yabe, T. et al. Demonstrated fossil-fuel-free energy cycle using magnesium and laser. *Appl. Phys. Lett.* **89**, 261107 (2006).
10. Mohamed, M. S. et al. Laser-induced magnesium production from magnesium oxide using reducing agents. *J. Appl. Phys.* **104**, 113110 (2008).
11. Kiss, Z. J., Lewis, H. R. Jr. & R., C. D. Sun pumped continuous optical maser. *Appl. Phys. Lett.* **2**, 93–94 (1963).
12. Nechayev, S. & Rotschild, C. Detailed balance limit of efficiency of broadband-pumped lasers. *Sci. Rep.* **7**, 11497 (2017).
13. Reusswig, P. D. et al. A path to practical solar pumped lasers via radiative energy transfer. *Sci. Rep.* **5**, 14758 (2015).

14. Dinh, T. H., Ohkubo, T., Yabe, T. & Kuboyama, H. 120 watt continuous wave solar-pumped laser with a liquid light-guide lens and an Nd:YAG rod. *Opt. Lett.* **37**, 2670 (2012).
15. Liang, D. & Almeida, J. Highly efficient solar-pumped Nd:YAG laser. *Opt. Express* **19**, 26399–26405 (2011).
16. Almeida, J., Liang, D., Guillot, E. & Abdel-Hadi, Y. A 40 W cw Nd:YAG solar laser pumped through a heliostat: a parabolic mirror system. *Laser Phys.* **23**, 065801 (2013).
17. Yabe, T. et al. High-efficiency and economical solar-energy-pumped laser with Fresnel lens and chromium codoped laser medium. *Appl. Phys. Lett.* **90**, 261120 (2007).
18. Mizuno, S., Ito, H., Hasegawa, K., Suzuki, T. & Ohishi, Y. Laser emission from a solar-pumped fiber. *Opt. Express* **20**, 5891 (2012).
19. Nsengiyumva, W., GuoChen, S., Hu, L. & Chen, X. Recent advancements and challenges in solar tracking systems (STS): a review. *Renew. Sustain. Energy Rev.* **81**, 250–279 (2018).
20. Press, W. H. Theoretical maximum for energy from direct and diffuse sunlight. *Nature* **264**, 734–735 (1976).
21. Nechayev, S., Reusswig, P. D., Baldo, M. A. & Rotschild, C. Designing a broadband pump for high-quality micro-lasers via modified net radiation method. *Sci. Rep.* **6**, 38576 (2016).
22. Swanson, R. M. The promise of concentrators. *Prog. Photovolt. Res. Appl.* **8**, 93–111 (2000).
23. Jin, K. & Zhou, W. Wireless laser power transmission: a review of recent progress. *IEEE Trans. Power Electron.* **34**, 3842–3859 (2019).
24. Zhang, I. et al. Distributed laser charging: a wireless power transfer approach. *IEEE Internet Things* **5**, 3853–3864 (2018).
25. Motohiro, T. et al. Concept of the solar-pumped laser-photovoltaics combined system and its application to laser beam power feeding to electric vehicles. *Jpn. J. Appl. Phys.* **56**, 08MA07-01–08MA07-06 (2017).
26. Sprangle, P., Hafizi, B., Ting, A. & Fisher, T. High-power lasers for directed-energy appliations. *Appl. Opt.* **54**, F201–F209 (2015).
27. Masuda, T., Iyoda, M., Yasumatsu, Y. & Endo, M. Low-concentrated solar-pumped laser via transverse excitation fiber-laser geometry. *Opt. Lett.* **42**, 3427–3430 (2017).
28. Bisson, J. -F., Iyoda, M., Yasumatsu, Y., Endo, M. & Masuda, T. Effect of the thermally excited lower laser level in a neodymium-doped fiber. *J. Optical Soc. Am. B* **36**, 736–745 (2019).
29. Masuda, T., Iyoda, M., Yasumatsu, Y. & Endo, M. Low-loss pigtail reflector for fiber lasers. *Rev. Sci. Instrum.* **88**, 053112 (2017).
30. Rigrod, W. W. Saturation effects in high-gain lasers. *J. Appl. Phys.* **36**, 2487 (1965).
31. Rigrod, W. W. Homogeneously broadened cw lasers with uniform distributed loss. *IEEE J. Quantum Electron.* **14**, 377–381 (1978).
32. Carroll, D. L. Effects of a nonhomogeneous gain saturation law on predicted performance of a high-gain and a low-gain laser systems. *Appl. Opt.* **33**, 1673–1681 (1994).
33. Endo, M., Bisson, J. -F. & Masuda, T. Monte carlo simulation of a transversely excited solar-pumped fiber laser. *Jpn. J. Appl. Phys.* **58**, 112006 (2019).
34. Ding, C. et al. Photoexcited hot and cold electron and hole dynamics at FAPbI3 perovskite quantum dots/metal oxide heterojunctions used for stable perovskite quantum dot solar cells. *Nano Energy* **67**, 104267 (2019).
35. CS, E. et al. Zero-reabsorption doped-nanocrystal luminescent solar concentrators. *ACS Nano* **8**, 3461–3467 (2014).
36. Masuda, T. et al. Solar-pumped fiber laser with all-inorganic cesium lead halide perovskite quantum dots. *Fiber Lasers XVI: Technol. Syst.* **10897**, 1089710 (2019).
37. Liu, F. et al. Highly luminescent phase-stable CsPbI3 perovskite quantum dots achieving near 100% absolute photoluminescence quantum yield. *ACS Nano* **11**, 10373–10383 (2017).
38. Jauregui, C., Limpert, J. & Tünnermann, A. High-power fibre lasers. *Nat. Photon.* **7**, 861–867 (2013).

Author contributions

T.M., J.F.B., and M.E. designed and fabricated the SPL laser devices. M.E. developed the Monte Carlo simulations and conducted the calculations. S.D., I.A.H., and B.S.R. conceived the idea for the liquid-phase LSC, and supported its design and simulation. T.M., J.F.B., and M.E. conceived the experiments. T.M., M.I., Y.Y., and M.E. conducted the measurements. M.E. supervised the experiments. T.M. wrote the manuscript with contributions from all authors. All authors discussed the results and commented on the manuscript.

Competing interests

The authors declare no competing interests.

Additional information